

Earth's Future

RESEARCH ARTICLE

10.1029/2024EF004737

Special Collection:

Regional Sea Level Change and Society

Key Points:

- We show that autonomous salinization is a key process driving salinization of low-lying coastal groundwater systems
- We find that sea-level rise and land subsidence are other major factors amplifying future groundwater salinization
- We describe how salinization of coastal fresh groundwater impacts different water users

Correspondence to:

S. L. Seibert,
stephan.seibert@uol.de

Citation:

Seibert, S. L., Greskowiak, J., Oude Essink, G. H. P., & Massmann, G. (2024). Understanding climate change and anthropogenic impacts on the salinization of low-lying coastal groundwater systems. *Earth's Future*, 12, e2024EF004737. <https://doi.org/10.1029/2024EF004737>

Received 28 MAR 2024
Accepted 22 JUN 2024





Author Contributions:

Conceptualization: Stephan L. Seibert, Janek Greskowiak, Gualbert H. P. Oude Essink, Gudrun Massmann
Formal analysis: Stephan L. Seibert
Funding acquisition: Gudrun Massmann
Investigation: Stephan L. Seibert
Methodology: Stephan L. Seibert
Project administration: Gudrun Massmann
Software: Stephan L. Seibert, Janek Greskowiak, Gualbert H. P. Oude Essink
Supervision: Janek Greskowiak, Gudrun Massmann
Validation: Stephan L. Seibert
Visualization: Stephan L. Seibert
Writing – original draft: Stephan L. Seibert

© 2024. The Author(s).

This is an open access article under the terms of the [Creative Commons Attribution License](#), which permits use, distribution and reproduction in any medium, provided the original work is properly cited.

Understanding Climate Change and Anthropogenic Impacts on the Salinization of Low-Lying Coastal Groundwater Systems

Stephan L. Seibert^{1,2} , Janek Greskowiak^{1,2} , Gualbert H. P. Oude Essink^{3,4} , and Gudrun Massmann^{1,2} 

¹Institute of Biology and Environmental Sciences, Carl von Ossietzky Universität Oldenburg, Oldenburg, Germany, ²Institute for Chemistry and Biology of the Marine Environment (ICBM), Carl von Ossietzky Universität Oldenburg, Oldenburg, Germany, ³Unit Subsurface and Groundwater Systems, Utrecht, The Netherlands, ⁴Department of Physical Geography, Utrecht University, Utrecht, The Netherlands

Abstract Fresh coastal groundwater is a valuable water resource of global significance, but its quality is threatened by saltwater intrusion. Excessive groundwater abstraction, sea-level rise (SLR), land subsidence and other climate-related factors are expected to accelerate this process in the future. The objective of this study is to (a) quantify the impact of projected climate change and (b) explore the role of individual hydrogeological boundaries on groundwater salinization of low-lying coastal groundwater systems until 2100 CE. We employ numerical density-dependent groundwater flow and salt transport modeling for this purpose, using Northwestern Germany as a case. Separate model variants are constructed and forced with climate data, that is, projected SLR and groundwater recharge, as well as likely ranges of other hydrogeological boundaries, including land subsidence, abstraction rates and drain levels. We find that autonomous salinization in the marsh areas, resulting from non-equilibrium of the present-day groundwater salinity distribution with current boundary conditions, is responsible for >50% of the salinization increase until 2100 CE. Sea-level rise, land subsidence and drain levels are the other major factors controlling salinization. We further show that salinization of the water resources is a potential threat to coastal water users, including water suppliers and the agrarian sector, as well as coastal ecosystems. Regional-scale uplifting of drain levels is identified as an efficient measure to mitigate salinization of deep and shallow groundwater in the future. The presented modeling approach highlights the consequences of climate change and anthropogenic impacts for coastal salinization, supporting the timely development of mitigation strategies.

Plain Language Summary Our study focuses on fresh groundwater near coastlines, which is crucial for drinking water, agriculture, and natural ecosystems, but is at risk of becoming salty due to mixing with saline groundwater. We investigate how climate change, including sea-level rise, changing groundwater recharge and subsiding land surfaces, might make this problem worse by 2100 CE. Northwestern Germany, located at the North Sea, is used as a case, and numerical groundwater models are employed to simulate the groundwater development in the study area. We find that the current groundwater salinity distribution is not at equilibrium with present-day boundary conditions, which is a primary reason for an expected salinity increase by 2100 CE. Rising sea-levels and the design of the marsh drainage system are other key factors. We show that raising mainland drainage levels would be an effective way to reduce future salinization in both deep and shallow groundwater. The methods applied in this study could help other coastal areas to understand the implications of future groundwater salinization.

1. Introduction

Low-lying coastal areas belong to the most densely populated regions of the world (Small & Nicholls, 2003). Water demands in these regions are often satisfied by groundwater abstraction (Minderhoud et al., 2020; Van Engelen et al., 2022). Yet, groundwater salinization (termed “salinization” in the following) is a major concern for the management of coastal groundwater systems (Karrasch et al., 2023; Oude Essink, 2001). Salinization has negative and long-lasting consequences for drinking water production and human health (Vineis et al., 2011), surface water quality (De Louw et al., 2010) as well as ecosystem health (Herbert et al., 2015). It can either be caused by overwash processes due to floodings during storm surges and subsequent infiltration of saltwater (Cantelon et al., 2022; Paldor & Michael, 2021) or (subsurface) saltwater intrusion (Werner et al., 2013). While

Writing – review & editing: Stephan L. Seibert, Janek Greskowiak, Gualbert H. P. Oude Essink, Gudrun Massmann

floodings are well-perceived, accompanied by severe damages (Tiggeloven et al., 2020) and linked to rapid aquifer salinization (Ataie-Ashtiani et al., 2013; Illangasekare et al., 2006), saltwater intrusion is a non-visible and much slower process. The physical driver of saltwater intrusion is a hydraulic head gradient from the sea toward the land. Factors controlling coastal head gradients and, thereby, saltwater intrusion are local sea-levels, ground surface elevations, drainage measures, groundwater recharge and groundwater abstraction.

Global climate change is expected to change some of the controlling factors of salinization within the 21st century. Firstly, global mean sea-levels will likely reach 0.44 (0.33–0.62; SSP1-2.6) m to 0.77 (0.63–1.01; SSP5-8.5) m above present-day mean sea-level (masl) at the end of the century (IPCC, 2021). Secondly, coastal land subsidence resulting from sediment compaction and groundwater abstraction will amplify relative sea-level rise (SLR), at least in some coastal regions (Minderhoud et al., 2020; Nicholls et al., 2021; Shirzaei et al., 2021). Thirdly, global fresh (ground-)water availability will shift in the future due to an expected variation of (inter-annual) groundwater recharge patterns (Döll, 2009; Portmann et al., 2013) as well as growing water demands (Wada & Bierkens, 2014). Because ~70% of the world's coastlines are topography controlled and, hence, the freshwater head cannot rise in response to hydrogeological boundary changes (Michael et al., 2013), rising sea-levels, subsiding land surfaces as well as changing groundwater recharge are expected to increase hydraulic sea-to-land head gradients and intensify coastal salinization.

SLR was found to be a major salinization driver in numerical density-dependent groundwater flow and salt transport modeling studies. For example, Oude Essink et al. (2010) reported >40% higher salt loads to surface waters for the low-lying Dutch Delta until the end of 21st century due to SLR. Also, Meyer et al. (2019) showed that SLR intensified salinization in the investigated Danish low-lying coastal groundwater system until the end of this century. Zamrsky et al. (2024) showed that, based on modelling 1,200 coastal regions, coastal areas could lose more than 5% of fresh groundwater by 2100 due to SLR, possibly affecting up to 60 million people. Groundwater drainage is another important salinization driver (Colombani et al., 2015; Feseker, 2007). The role of drainage-induced salinization was recently quantified in a preceding study by Seibert et al. (2023), where the establishment of a dense drainage system accelerated coastal salinization in Northwestern Germany over the past centuries. Oude Essink et al. (2010) showed that the effects of land subsidence can possibly even exceed the negative effects of SLR. Groundwater abstraction was identified as major salinization driver in some other studies. For instance, Ferguson and Gleeson (2012) stated that groundwater salinization at the USA coast is largely driven by abstraction under a wide range of hydrogeologic conditions, while SLR has a higher impact only in regions with low hydraulic gradients. Similarly, Green and MacQuarrie (2014) found that abstraction was the primary salinization driver close to well fields in a coastal sandstone aquifer in Atlantic Canada.

Although our understanding of coastal salinization has advanced over the past decades, regional modeling studies integrating time-resolved climate data, such as SLR, recharge and land subsidence projections, are lacking. The simulation of variable-density groundwater flow and salt transport driven with hydrogeological data for climate scenarios is, however, required to obtain ranges of expected future salinization. Furthermore, systematic investigations regarding the role of individual hydrogeological parameters and boundaries are needed to understand which hydrogeological processes dominate coastal salinization.

The objectives of this paper are to (a) study the effect of future climate change on salinization of low-lying coastal areas and (b) assess the relevance of individual hydrogeological parameters and boundaries as salinization drivers. For this purpose, large-scale numerical density-dependent groundwater flow and salt transport modeling was applied to a case study area in Northwestern Germany. The study site is representative for sandy low-lying coastal regions in Northern Europe, which are often characterized by permeable Pleistocene and Holocene sediments and a dynamic history of coastal development. The present-day salinity distribution was derived in a previous study that integrated a comprehensive paleo-modeling approach (Seibert et al., 2023). Findings of our work highlight the major consequences of projected climate change as well as anthropogenic impacts for salinization of groundwater resources in low-lying coastal areas.

2. Materials and Methods

2.1. Site Description

The study area is located in Northwestern Germany and characterized by low-lying marshes with elevations around or below present-day mean sea-level (masl) and a more elevated glacial landscape (so called “geest”) with

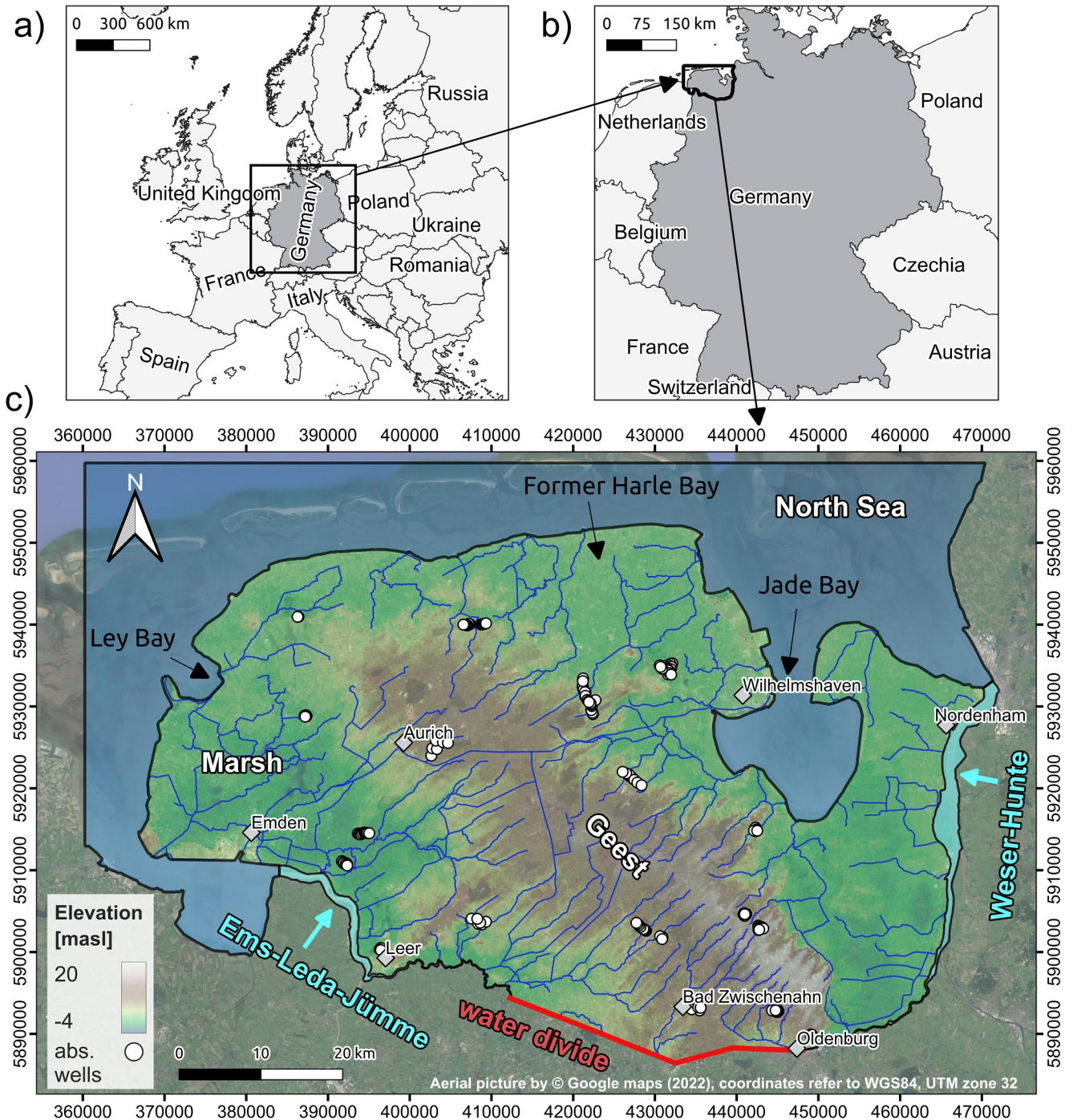


Figure 1. Location of the study area in panel (a) Europe and (b) Germany. (c) Study area outlined in panel (b). Thin blue lines in panel (c) indicate the location of rivers (NLWKN, 2016). White symbols mark the location of production wells operated by the water suppliers. The elevation model shown in panel (c) is based on BKG (2013). The major rivers “Ems-Leda-Jümme” and “Weser-Hunte” were defined as Dirichlet-type (first-type) boundaries. The “water divide” as well as the margins of the North Sea act as no flow boundaries.

a maximum elevation of ~ 20 masl (Figure 1). The river networks Ems-Leda-Jümme and Weser-Hunte, the North Sea as well as a water divide delineate the study area to the west, east, north and south, respectively. A dense network of drains and ditches was established in the low-lying marshes over the past centuries, which controls surface and groundwater levels (Seibert et al., 2023). Groundwater abstraction for drinking water production takes place in the geest by 16 local water works, producing in total ~ 60 million m^3 of drinking water (Mm^3) per

year. Additional groundwater abstraction, for example, by industry and agriculture, is assumed to be comparatively small and was not regarded in this study due to lacking data.

2.1.1. Geology and Geomorphology

The groundwater system is characterized by unconsolidated sediments, which originate from the geological periods Tertiary and Quaternary. Low-pervious Miocene silty-clayey sediments form the aquifer base. Permeable sands and gravel deposits from Late Miocene, Pliocene and Pleistocene lay on top of the impermeable base and act as aquifers. Tertiary and Pleistocene clayey, low-pervious material is locally embedded in the groundwater system and acts as aquitards. The top sediments of the marsh area are characterized by fine sands, silt, clay and peat deposits, which accumulated during the Holocene. Glaciation and marine transgression shaped the geology and geomorphology in the study area during the Pleistocene and Holocene (Karle et al., 2021). More detailed descriptions of the geology, the paleogeography and the coastline evolution are presented in Seibert et al. (2023), who simulated the paleo-evolution of groundwater in the study area.

2.1.2. Hydrology and Hydrogeology

The present-day annual precipitation corresponds to $\sim 823 \text{ mm a}^{-1}$ (mean 1981–2010, DWD station 5839 “Emden,” DWD, 2021), and the average groundwater recharge is $\sim 270 \text{ mm a}^{-1}$ (mGROWA22, Ertl et al., 2019). Highest recharge rates are found in the geest region, whereas marsh recharge is limited due to drainage measures. The present-day head and salinity distributions in the investigated groundwater system were re-constructed in a previous paleo-modeling study (Seibert et al., 2023), that showed that SLR and paleogeographic changes linked to marine transgression were dominant factors driving salinization during most of the Holocene. Yet, coastline and topography changes as well as groundwater drainage linked to land cultivation accelerated salinization since ~ 1600 Common Era (CE).

2.2. Modeling Approach

Numerical variable-density groundwater flow and salt transport modeling (termed “modeling” in the following) was applied to study the effect of climate change and individual model parameters on future salinization of low-lying coastal areas. The general modeling approach and used input data are explained in the following. More information on model discretization and set-up of model boundaries is provided in Section 2.3. A detailed description regarding the construction of the basic model and its boundaries can also be found in Seibert et al. (2023), which followed a similar modeling approach but focused on paleo salinization, hence, covered a different time span and used different input data.

The software package iMOD-WQ (Verkaik et al., 2021), a parallelized version of SEAWAT V4 (Langevin et al., 2008), which couples the software packages MODFLOW-2000 (Harbaugh et al., 2000) and MT3DMS (Zheng & Wang, 1999), was used for the numerical simulations. The script-based software package iMOD-Python (Visser & Bootsma, 2019) was employed for generation of model input files to iMOD-WQ. All numerical simulations were run on the high-performance cluster “ROSA” at the University Oldenburg.

566 separate 3-D model variants of the study area were constructed to (a) evaluate the effect of autonomous salinization resulting from non-stationarity of the groundwater system with present-day hydrogeological boundary conditions (so-called Model Base Case, MBC; $n = 1$), (b) simulate future salinization with projected input data (so-called PRO model variants; $n = 456$) and (c) systematically explore the role of individual model parameters (so-called LIN model variants; $n = 109$) (Table 1). All model variants covered a simulation time of 80 years to obtain the future salinity distribution at 2100 CE, using 2020 CE as the starting point. The length of simulation periods in which model boundary conditions remained constant, so-called stress periods in MODFLOW terminology, had a length of 10 years. Boundary changes, for example, SLR, took place incrementally between stress periods, thus, in eight steps from 2020 CE until 2100 CE. The initial conditions, that is, the situation at 2020 CE, of the head and salinity distributions in the study area corresponded to the final head and salinity distributions simulated for “Model BC” in the study Seibert et al. (2023). Note that Model BC in Seibert et al. (2023) was used to reconstruct the salinity distribution during the Holocene until 2020 CE, that is, the last 9,000 years, considering relevant hydrogeological changes, for example, paleo SLR, paleogeographic development, surface elevation and coastline changes, artificial drainage and groundwater abstraction.

Table 1
Overview of the Modeling Approach

Model subset	Aim	Set-up of model variants	No. of variants (n)
MBC	Evaluation of autonomous salinization	<ul style="list-style-type: none"> Application of present-day boundary conditions 	1
PRO	Projection of future salinization	<ul style="list-style-type: none"> Sea-levels^a: 5, 17, 50, 83, 95, 99.5 percentiles for RCP-2.6 ($n = 6$) and RCP-8.5 ($n = 6$) Recharge^b: ensemble members of RCP-2.6 ($n = 8$) and RCP-8.5 ($n = 11$) Land subsidence: 0, 3, 6, 12 mm a⁻¹ ($n = 4$) 	456
LIN	Evaluation of individual model boundaries	<ul style="list-style-type: none"> Change of individual model boundaries, that is, sea-level, drainage, recharge, land subsidence, abstraction (compare Table 2) 	109

Note. For RCP-2.6 PRO model variants, six percentiles of projected sea-levels, eight ensemble members of projected recharge and four land subsidence assumptions were regarded, yielding a total combination of $n = 192$ separate models. For RCP-8.5 PRO model variants, six percentiles of projected sea-levels, 11 ensemble members of projected recharge and four land subsidence assumptions were regarded, yielding a total combination of $n = 264$ separate models. ^aSLR projections for tide gauge Cuxhaven from Kopp et al. (2014). ^bmGROWA18/22 data based on Herrmann et al. (2013), Hajati et al. (2022) and LBEG and NIKO (2022).

Present-day boundary conditions remained unchanged in MBC. This model variant served as a baseline simulation to quantify salinization resulting from non-stationarity of the hydrogeologic system with present-day boundary conditions (termed “autonomous salinization” in the following). Furthermore, note that the small SLR from 2000 to 2020 CE (<0.25 m for all scenarios, Figure 2) was neglected in MBC, and a steady sea-level of 0 masl was assumed instead for this period. The PRO model variants were forced with sea-levels projected for the tide gauge Cuxhaven by Kopp et al. (2014). Sea-levels for 5, 17, 50, 83, 95 and 99.5 percentiles of RCP-2.6 and RCP-8.5 scenarios, respectively, for the years 2030, 2050 and 2100 CE (Kopp et al., 2014), were used and linearly interpolated to obtain decadal estimates of future sea-levels (Figure 2). Note that the SLR projections regarded background subsidence, which corresponded to 1.0 ± 0.2 mm a⁻¹ at tide gauge Cuxhaven (Kopp et al., 2014). Projected groundwater recharge rates were derived from the federal state hydrologic model mGROWA22, which provides regional climate projection data for the federal states Lower Saxony and Bremen (AR5-NI v2.1) (Hajati et al., 2022; Herrmann et al., 2013; LBEG and NIKO, 2022). For the purpose of this study, annual recharge projections of 8 (RCP-2.6) and 11 (RCP-8.5) mGROWA22 ensemble members were used to calculate spatially

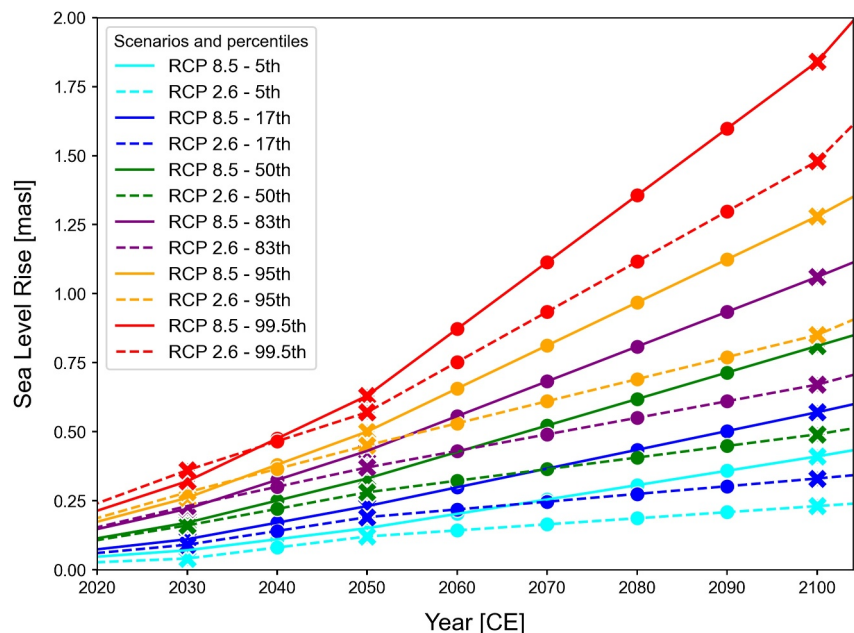


Figure 2. Projected sea-levels for tide gauge Cuxhaven, North Sea. Data for the years 2030, 2050 and 2100 (crosses) was obtained from Kopp et al. (2014). Values between these years were derived via linear interpolation (dots). The projected sea-levels were applied to the sea boundary in the different model variants, employing eight so-called “stress periods” in MODFLOW terminology.

Table 2
Set-Up of LIN Model Variants

Model boundary	Unit	Value MBC	Unit change	Change compared to MBC			Model variants (n)
				Min.	Max.	Δ	
Sea-level	masl	0	masl	+0.1	+2.0	0.1	20
Drainage	mbgs	0.8 to 1.0 ^a	mbgs	-2.0	+1.0	0.1	30
Recharge	mm a ⁻¹	~270 ^b	%	-90	+100	10	19
Subsidence	m	0	m	+0.1	+2.0	0.1	20
Abstraction	Mm ³ a ⁻¹	~60	%	-100	+100	10	20

Note. “Min.” and “Max.” correspond to the minimum and maximum change, respectively, considered for the corresponding boundary. “Δ” corresponds to the incremental change between the n model variants simulated for the considered boundary. “mbgs” abbreviates meter below ground surface. ^aLocally varying drainage depths were implemented according to Ertl et al. (2019). ^bAnnual mean recharge for the reference period 1981 to 2010 (mGROWA18; Ertl et al., 2019).

resolved decadal mean recharge values for each ensemble member. Note that each PRO model variant representing a specific percentile of a SLR scenario was forced with all available recharge ensemble members, employing separate model variants. For instance, 11 separate PRO model variants were simulated for the 95 percentile of the SLR RCP-8.5 scenario. RCP-2.6 and RCP-8.5 scenarios were chosen for SLR and groundwater recharge projections to cover the likely range between a more optimistic and a business-as-usual scenario.

Moreover, spatially resolved land subsidence resulting from peat oxidation and clay shrinkage was accounted for in a subset of PRO model variants, which came on top of the background subsidence rate of ~1 mm a⁻¹ already lumped into the local SLR projections. For this purpose, constant land subsidence rates of 3, 6 and 12 mm a⁻¹, respectively, were applied over the entire simulation period at all locations characterized by Holocene clay, silt or peat, regardless of the depth of the respective deposits. Thus, PRO model variants regarding spatially resolved land subsidence accounted for subsidence twice, because SLR projections by Kopp et al. (2014) also considered background subsidence. However, we were particularly curious about the local effect of land subsidence, that is, concerning land subsidence at spatially resolved locations, which was not possible when only regarding background subsidence lumped into SLR projections. Furthermore, we wanted to test the effect of more drastic land subsidence rates >1 mm a⁻¹ on salinization, which is realistic considering reported land subsidence rates of up to >10 mm a⁻¹, for example, for the neighboring low-lying coastal region in the Netherlands (Oude Essink et al., 2010). In the following, the term land subsidence refers to the spatially resolved land subsidence related to Holocene sediment compaction, rather than comparatively low background subsidence lumped into SLR projections.

Note that surface elevation grids were re-constructed for each stress period of all model variants considering land subsidence, which served as elevation information for the drain and river boundaries. Unfortunately, spatially resolved land subsidence projections were not available for the study area, but the uniformly applied rates fall into the range of land subsidence reported for other coastal regions (e.g., Herrera-García et al., 2021; Minderhoud et al., 2020; Nicholls et al., 2021). The integrated land subsidence assumption is certainly a simplification, for example, considering that the actual thickness of Holocene clay, silt and peat deposits was not regarded, and future work should explore the effect of local land subsidence on salinization based on more sophisticated land subsidence models.

The LIN model variants explored the individual effects of SLR, drain elevation, groundwater recharge, land subsidence and groundwater abstraction on salinization, changing one parameter at a time in each model variant (Tables 1 and 2). SLR, groundwater recharge and land subsidence changed linearly from 2020 CE until 2100 CE in LIN variants, using the values in Table 2 as final values in 2100 CE, whereas variations of drain elevation and abstraction rates (Table 2) were deployed immediately in LIN variants and remained constant throughout the simulation period.

2.3. Model Discretization and Boundaries

The groundwater system was represented by a regular grid (160 rows, 240 columns, 120 layers) with a total of ~2.1 million active model cells. Horizontal and vertical spacing between grid nodes were 500 and 2 m,

respectively. Top and bottom elevations of the uppermost and lowest model layer corresponded to 20 and -220 masl. Effective porosity as well as longitudinal, transverse horizontal and transverse vertical dispersivity were set to 0.25 and 2 m, 0.2 and 0.02 m, respectively, which are common values for unconsolidated large-scale coastal groundwater systems (e.g., Delsman et al., 2014; Meyer et al., 2019; Oude Essink et al., 2010; Van Engelen et al., 2019).

The employed geologic model was based on three separate regional geologic models (LBEG, 2018; OOWV, 2020). Geologic layer information was carefully reviewed and transferred into hydrostratigraphic units, following Reutter (2013). Hydraulic conductivities of both aquifers and aquitards, which are important parameters for the variable-density groundwater flow and salt transport models, were derived for relevant hydrostratigraphic units, using the parameter estimation software PEST (Doherty, 2021a, 2021b). Present-day groundwater head and discharge data served as calibration data. The model calibration procedure including estimated parameter values is explained in detail in Seibert et al. (2023).

Interaction with the sea was regarded using a so-called Robin-type head-dependent flux boundary (third-type General Head Boundary, GHB). Sea-levels were applied as external heads for the GHB boundary of the model variants. Inflow from the sea boundary had a salinity of 35 g TDS L^{-1} . Groundwater recharge was applied using a so-called Neumann-type constant-flux boundary (second-type boundary). Present-day groundwater recharge was based on the annual average for the period 1981–2010 of the Lower Saxony federal state hydrologic model mGROWA18 (Ertl et al., 2019) and used for all LIN variants. Recharge projections of mGROWA22 AR5-NI v2.1 (Section 2.2) were employed in the PRO variants. The effect of land subsidence (Section 2.2) was accounted for by decreasing ground surface elevations at locations where Holocene clay and peat deposits were present. Land subsidence had a direct impact on drain and river levels, as they were coupled to the ground surfaces.

Groundwater drainage was regarded using a third-type boundary. Drainage locations and depths were obtained from Ertl et al. (2019), and a model-wide MODFLOW drain conductance of $0.45 \text{ m}^2 \text{ d}^{-1} \text{ m}^{-2}$ was used (Seibert et al., 2023). Note that the provided spatially resolved drain elevations were instantaneously and uniformly increased/lowered in LIN model variants, applying the drain elevation values presented in Table 2. Groundwater abstraction via 170 pumping wells (white circles, Figure 1) was implemented using a second-type boundary. Rivers in the mainland (blue lines, Figure 1) were regarded as third-type boundary, applying calibrated river properties from Seibert et al. (2023). Note that we assumed freshwater salinity for the latter type of rivers, because they are typically protected from seawater inflow due to the presence of floodgates. Meanwhile, we recognize that the effect of surface water salinity on coastal groundwater salinization (Smith & Turner, 2001) can be significant in other coastal zones, like the Ganges-Brahmaputra-Meghna and Mekong deltas, respectively (Bhuiyan & Dutta, 2012; Eslami et al., 2019). Therefore, saline surface waters should be regarded via corresponding model boundaries under such circumstances. The two major rivers Ems and Weser (Figure 1c) were implemented as so-called Dirichlet-type boundary (first-type boundary with time-variant specified-head, CHD), using SLR-corrected present-day river levels and salinities (Seibert et al., 2023). The margins of the sea, the water divide in the south as well as the base of the groundwater system were regarded as no-flow boundaries.

2.4. Model Evaluation

Model results were evaluated with respect to different salinization descriptors, that is, future freshwater volumes, freshwater interface depths, volume and salinity of groundwater discharge to the surface water system, salt loads to the surface water system, near-surface electrical conductivity (EC) as well as seawater inflow rates. Freshwater volumes were calculated by (a) converting salinities of all model cells to chloride (Cl) concentrations, applying a factor of $526 \text{ mg Cl per g salt}$, based on the Cl ratio in seawater (Seibert et al., 2018), (b) summing up the number of fresh model cells in the mainland with Cl concentrations $<250 \text{ mg L}^{-1}$ and (c) multiplying the total number of fresh model cells with the water volume of a model cell, that is, $125,000 \text{ m}^3$, considering 500 m (dx and dy) and 2 m (dz) as cell dimensions and a porosity of 0.25. A Cl threshold of 250 mg L^{-1} was used to delineate freshwater interface depths. The volume of groundwater discharge to the surface water system was derived by summing up outflows via drain and river boundaries. Salt loads were calculated multiplying groundwater discharge volumes to surface waters by salt concentrations in discharging groundwater. Near-surface groundwater salinities reflect the salinity in the uppermost active model cell that covers the top two m of the groundwater system. Note that salinities were converted to electrical conductivity (EC, unit dS m^{-1}), assuming a conversion factor of 0.6768 (Holt

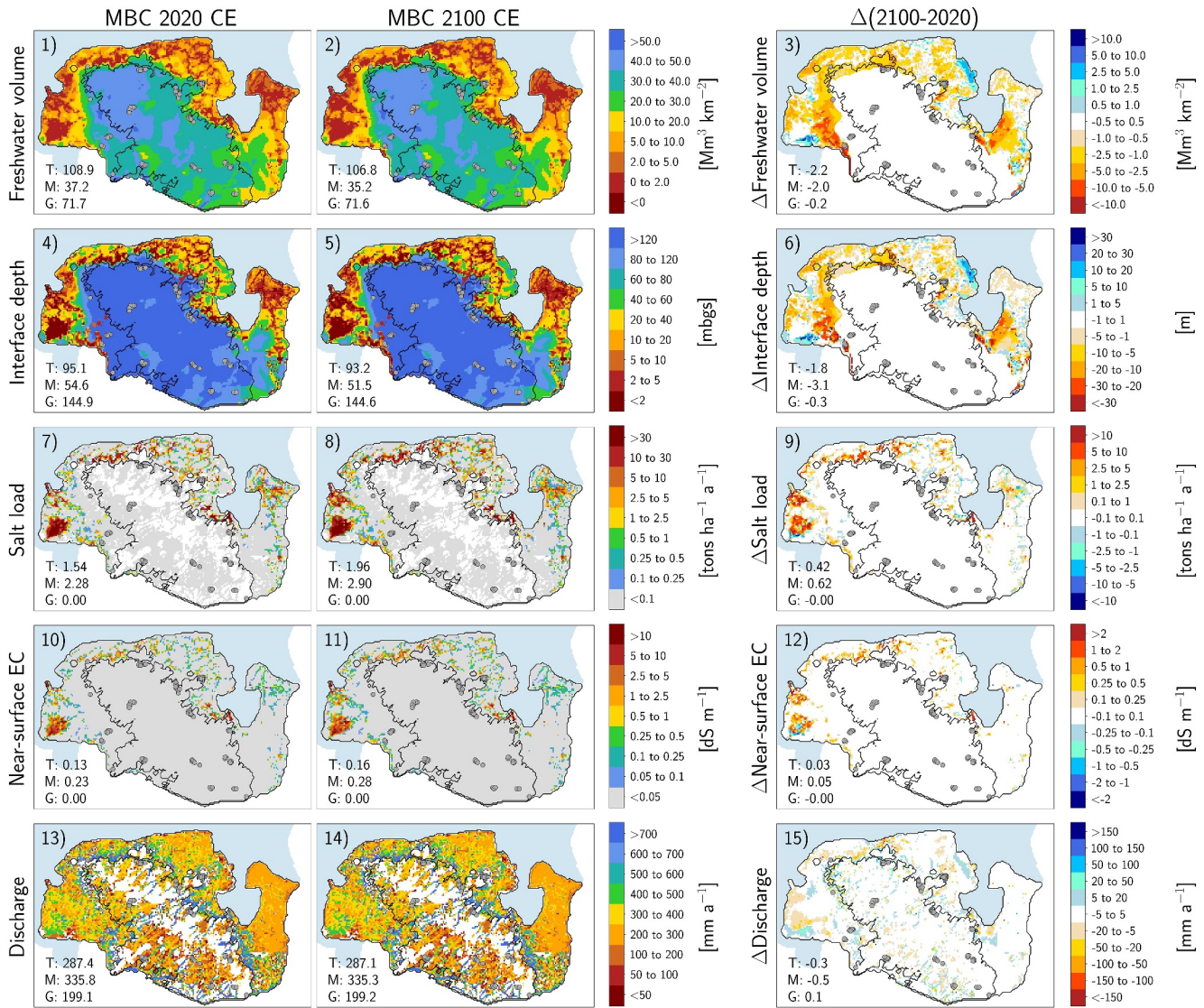


Figure 3. Fresh groundwater volumes (first row), freshwater interface depths (second row), salt loads (third row), near-surface groundwater salinities (fourth row, EC = electrical conductivity) and groundwater discharge to surface waters (fifth row) for MBC at 2020 CE (first column) and 2100 CE (second column). The third column presents the difference between 2020 CE and 2100 CE, that is, model results for 2020 CE were subtracted from model results for 2100 CE. Note that color legends are swapped in row 3 and 4 of column 3 compared to the remaining rows, ensuring that adverse changes resulting from salinization are presented in red. Total fresh groundwater volumes (km^3) as well as mean values for freshwater interface depths (mbgs), salt loads ($\text{tons ha}^{-1} \text{a}^{-1}$), near-surface EC (dS m^{-1}) and groundwater discharge to surface water (mm a^{-1}) are presented in the bottom left corner of each subplot in column one and two for the entire mainland (T), the marsh (M) and the geest (G). Values in the bottom left corner of subplots in column three indicate the difference between 2020 CE to 2100 CE.

et al., 2017). The seawater inflow rate per m coastline was calculated by summing up the inflow of seawater through the GHB boundary and dividing by the total coastline length, that is, ~ 246 km.

3. Results

3.1. Autonomous Salinization

The hotspot of present-day salinization in MBC (autonomous salinization model variant) was the low-lying marsh, which is characterized by low fresh groundwater volumes, freshwater interfaces that are close to the ground surface and high salt loads to surface waters as well as near-surface groundwater salinities (Figures 3-1, 3-4, 3-7, and 3-10). Autonomous salinization intensified these trends in the marsh until 2100 CE (Figures 3-2, 3-5,

3-8, and 3-11). In contrast, the elevated geest landscape was virtually not affected by present and/or future salinization in MBC.

The fresh groundwater volume decreased by ~5% (Figure 3-3) and the freshwater interface moved ~3.1 m upwards on average (Figure 3-6) in the marsh until 2100 CE in MBC. While these changes sound moderate, they correspond to an annual loss of ~25 and 2.5 Mm³ fresh groundwater in marsh and geest, respectively, which is a substantial fraction of the annual water demand of ~60 Mm³ by the regional water suppliers. Hence, autonomous salinization will uplift deeper saline groundwater in the future and, thereby, shift the freshwater interface closer to the ground surface even without any further SLR, change in groundwater recharge or land subsidence. Freshening in some parts of the study region, for example, western (Emden city), northern (former Harle Bay) and eastern (Wilhelmshaven region) areas, after 2020 CE resulted from coastline changes and embankment activities during the past centuries (Seibert et al., 2023).

Average present-day marsh salt loads corresponded to ~2.3 tons ha⁻¹ a⁻¹, although salt loads up to >30 tons ha⁻¹ a⁻¹ were locally observed (Figure 3-7), resulting from high seepage fluxes and near-surface salinities (Figures 3-10 and 3-13). The increase of average marsh salt loads and near-surface salinities due to autonomous salinization was +27% and +23%, respectively, until 2100 CE (Figures 3-9 and 3-12). Hotspots of present-day salt loads were also identified as locations receiving the highest additional salt loads in the future (Figures 3-7, 3-8, and 3-9). The reason for the rise of salt loads in MBC was the increase of near-surface salinities rather than the increase of discharge, which remained constant from 2020 to 2100 CE (Figures 3-13–3-15).

3.2. Effect of Future Climate Change

The projected climate change further contributed to the deterioration of coastal freshwater resources in PRO model variants (Figures 4 and 5). The faster the SLR, that is, greater increase of SLR for more pessimistic climate scenarios and larger percentiles, respectively, until 2100 CE, the more intense was the loss of fresh groundwater volume, the uplift of the freshwater interface as well as the increase of salt load and near-surface salinity in the marsh, respectively, compared to MBC (Figure 4, column one in Figure 5). For instance, the model variant for the 95 percentile of the RCP-8.5 scenario (second most pessimistic scenario in terms of SLR considered) showed a marsh fresh groundwater volume decrease of ~10% (Figure 5-1), an average marsh freshwater interface uplift of ~6 m (Figure 5-5) and more than a tripling of marsh average salt loads as well as a doubling of seawater inflow rates until 2100 CE (Figures 5-9 and 5-17) compared to present-day values if no land subsidence was assumed. A SLR of ~1.3 m until 2100 CE, corresponding to the 95 percentile of RCP-8.5, resulted in a marsh freshwater loss comparable to the one caused by autonomous salinization alone (Figure 3-3 vs. Figure 4-18). RCP-2.6 model variants showed similar but less drastic trends for all salinization parameters (Figure 5). Most severe changes were found for the 99.5 percentiles of both RCP scenarios, corresponding to an extreme SLR of 1.48 m (RCP-2.6) and 1.84 m (RCP-8.5) until 2100 CE, respectively. Accordingly, the model variants for the 99.5 percentile of the RCP-8.5 scenario showed a quadrupling of marsh salt loads and a tripling of average discharge salinities until 2100 CE (Figures 5-9 and 5-21). Notably, even the best-case SLR of ~0.2 m until 2100 CE (5 percentile of RCP-2.6) increased salinization in the marsh (first column in Figure 4) compared to MBC.

The loss of fresh groundwater volume and the upward movement of brackish and saline deeper groundwater was most pronounced at locations close to the coast (row one and two in Figure 4). On the other hand, the future increase of salt loads took place at the hotspots that were also affected by autonomous salinization in MBC (Figures 3-9 and row three in Figure 4). Salt loads in model variants for RCP-2.6 and RCP-8.5 increased in virtually the entire marsh (Figures 4-7–4-9 and 4-22–4-24). Model variants for the 5 percentiles of RCP-2.6 and RCP-8.5 locally demonstrated a decrease of near-surface salinities relative to MBC (blue areas in Figures 4-10 and 4-25), whereas model variants for 50 and 95 percentiles of both RCP scenarios showed a general increase of near-surface salinities (Figures 4-11, 4-12, 4-26, and 4-27). Note that the projected wetter climate, likely causing the aforementioned local freshening trends, was reflected by a simulated rise of future groundwater discharge to surface water in our models (Figure 5-25). An acceleration of the increase of marsh salt loads, near-surface salinities, discharge salinities as well as seawater inflow rates was observed after ~2050 CE (Figures 5-9, 5-13, 5-17, and 5-21), which is in line with the projected trends of SLR (Figure 2). The relative changes of fresh groundwater volume and interface depth were smaller and more linear from 2020 to 2100 CE (Figures 5-1 and 5-5). As an example, average marsh salt loads increased by up to >200% (Figure 5-9), while marsh fresh groundwater volumes decreased by up to >10% from 2020 CE until 2100 CE (Figure 5-1).

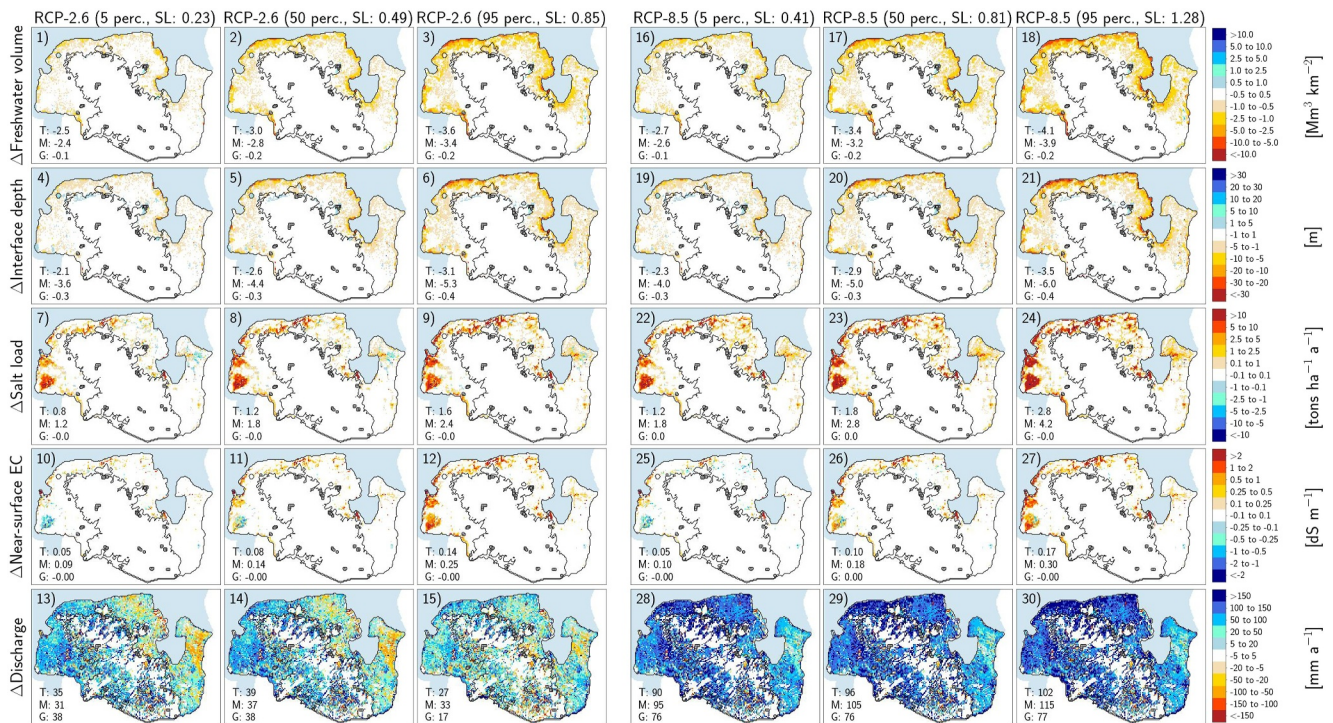


Figure 4. Impact of projected climate change on fresh groundwater volume (first row), freshwater interface depth (second row), salt load (third row), near-surface groundwater salinity (fourth row; EC = electrical conductivity) and groundwater discharge (fifth row) for selected PRO model variants at 2100 CE. Columns one to three and four to six show the differences of model variants for 5, 50 and 95 percentiles of RCP-2.6 and RCP-8.5, respectively, at 2100 CE compared to MBC at 2100 CE. No spatially-resolved-land-subsidence model variants are shown, and the presented model variants regarded the recharge projection ensemble member yielding the median relative salinity increase of all simulated recharge ensemble members for the respective percentile of SLR. The projected sea-level (SL) for the respective model scenario in 2100 CE is indicated in the column headings. The changes of fresh groundwater volume (km^3), mean freshwater interface depth (mbs), salt load ($\text{tons ha}^{-1} \text{a}^{-1}$), near-surface salinity (dS m^{-1}) and groundwater discharge to surface water (mm a^{-1}) from 2020 CE to 2100 CE are presented in the bottom left corner of each subplot for the entire mainland (T), the marsh (M) as well as the geest (G).

Land subsidence related to spatially resolved compaction of Holocene clay/peat/silt deposits amplified future salinization in our models (columns two to four in Figure 5). For instance, marsh salt loads increased from $\sim 6.5 \text{ tons ha}^{-1} \text{a}^{-1}$ in 2100 CE (95 percentile of RCP-8.5, Figure 5-9) to $>10 \text{ tons ha}^{-1} \text{a}^{-1}$ in 2100 CE for model variants taking a land subsidence rate of 12 mm a^{-1} into account (95 percentile of RCP-8.5, Figure 5-12). Even for model variants representing low percentiles of RCP-2.6, land subsidence caused a clear decrease of marsh fresh groundwater volume and interface depth as well as an increase of salt load, near-surface salinity, discharge salinity and seawater inflow rates (e.g., fourth column in Figure 5).

3.3. Role of Individual Model Boundaries

SLR, a lowering of drainage levels and land subsidence were the dominant drivers of salinization in LIN model variants (red, green and orange symbols in Figures 6 and 7). These factors resulted in an increase of seawater inflow into the groundwater system (Figure 6a), a decrease of the marsh fresh groundwater volume (Figures 6b and 7), a rise of marsh salt load (Figure 6b) and near-surface salinity (Figure 6c) as well as a lifting of marsh freshwater interfaces (Figure 6c). On the other hand, a variation of groundwater recharge (purple symbols in Figure 6) had only a small impact on the seawater inflow rate (Figure 6a), marsh fresh groundwater volume (Figure 6b) as well as the freshwater interface depth (Figure 6c). The almost linear relationship of groundwater discharge to surface water and the amount of applied recharge (Figure 6a, larger symbols indicate more recharge) underlines that the groundwater system is heavily controlled by drainage measures, which force the discharge of shallow groundwater. Moreover, the nearly linear relationship between marsh salt load and additional recharge (Figure 6b) demonstrates that salt fluxes were governed by both the increase of near-surface salinity, as shown for MBC, as well as the increase of discharge rates. The change of groundwater abstraction rates had virtually no impact on any of the investigated salinization descriptors on a regional scale (blue symbols in Figure 6).

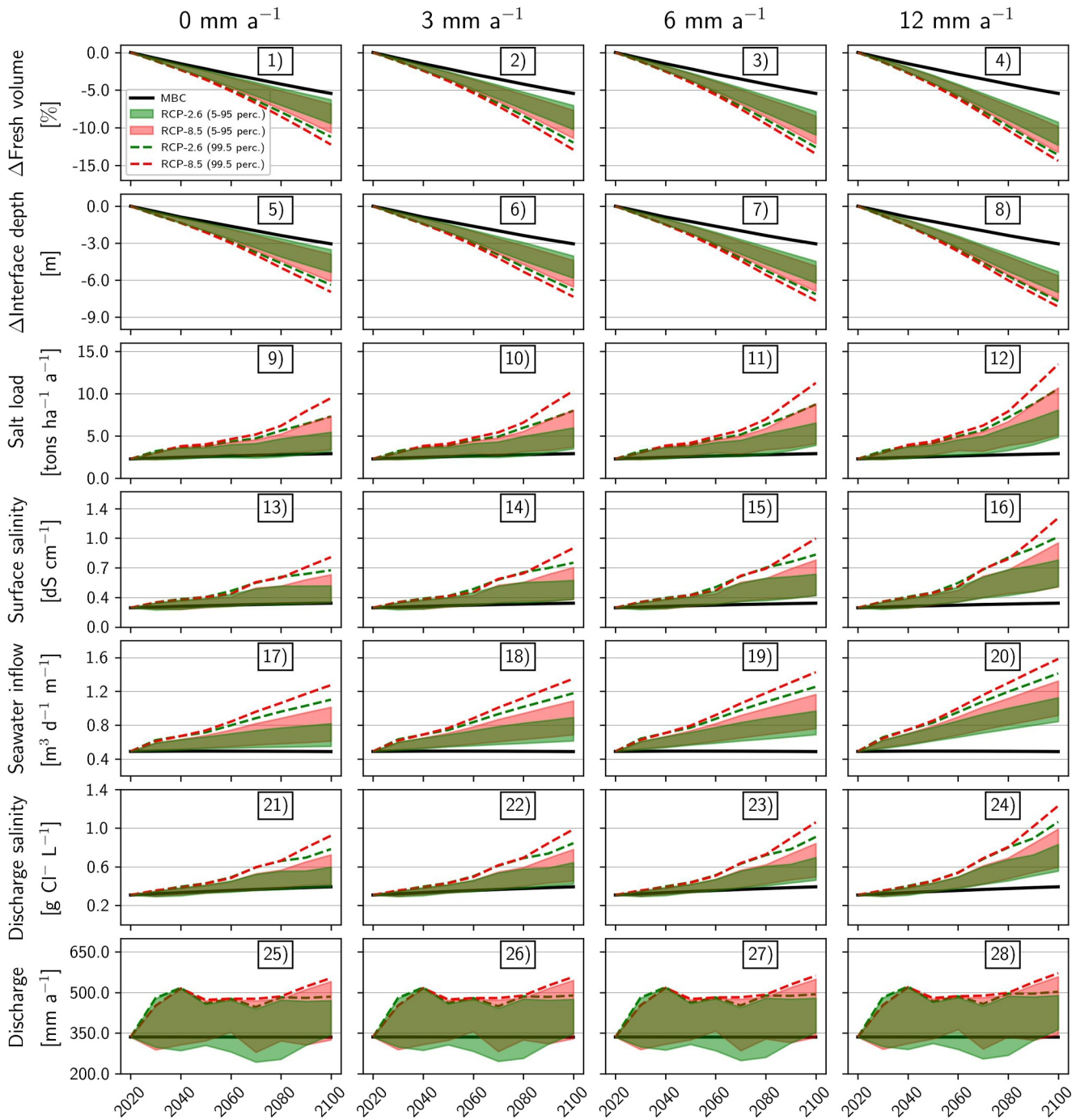


Figure 5. Temporal evolution of marsh fresh groundwater volume (row one) and average freshwater interface depth (row two) as well as average salt load (row three), near-surface salinity (row four), seawater inflow rate (row five), discharge Cl concentration (row six) and groundwater discharge to surface water rate (row seven). Columns one to four show results for the spatially resolved land subsidence scenarios related to compaction of Holocene clay/peat/silt deposits, assuming rates of 0, 3, 6 and 12 mm a⁻¹, respectively. Green and red colored areas mark results for model variants for 5 to 95 percentiles of RCP-2.6 and RCP-8.5 scenarios, respectively. Note that results for RCP-2.6 and RCP-8.5 scenarios partly overlap, indicated by khaki colored areas. Dotted green and red lines present results for model variants of 99.5 percentiles of RCP-2.6 and RCP-8.5 scenarios, respectively. The black line shows salinization trends of MBC.

Autonomous salinization caused a decrease of marsh fresh groundwater volume and freshwater interface depth by ~5% and ~3 m, respectively, from 2020 to 2100 CE (cross symbols in Figures 6b and 6c). Yet, it had no strong impact on the rate of seawater inflow and groundwater discharge to surface water (cross symbols in Figure 6a). Concerning future climate change, RCP-2.6 and RCP-8.5 PRO model variants (green and gray boxes in Figure 6

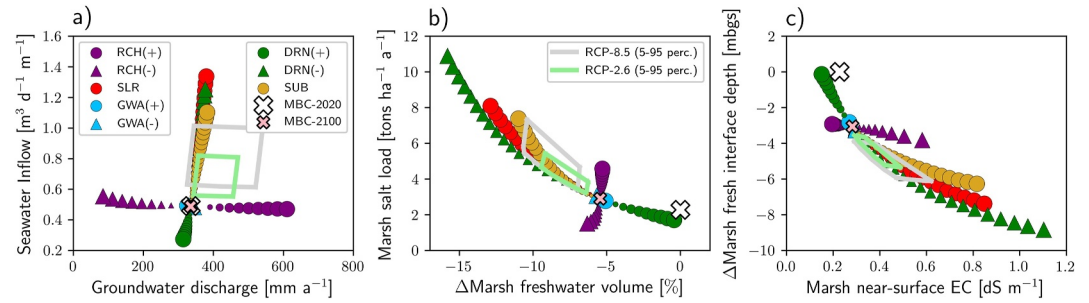


Figure 6. LIN model variants at 2100 CE. (a) Groundwater discharge to surface water versus seawater inflow into the groundwater system, (b) change of marsh fresh groundwater volume versus marsh salt load and (c) marsh near-surface electrical conductivity (EC) versus change of marsh freshwater interface depth. RCH(+), RCH(-), SLR, GWA(+), GWA(-), DRN(+), DRN(-) and SUB show results for LIN model variants with increased/decreased groundwater recharge, SLR, increased/decreased groundwater abstraction, increased/decreased drain elevation and spatially resolved land subsidence related to compaction of Holocene sediments, respectively (compare Table 2). The symbol size corresponds to the magnitude of change. Cross symbols mark the situations of MBC in 2020 CE (white) and 2100 CE (red), respectively. Green and gray boxes enclose all no-land-subsidence RCP-2.6 and RCP-8.5 PRO model variants (5–95 SLR percentiles), respectively, at 2100 CE.

enclose all no-spatially-resolved-land-subsidence RCP-2.6 and RCP-8.5 PRO model variants, respectively) plot close to LIN model variants exploring only SLR, which emphasizes that SLR was the major factor driving future salinization in the PRO model variants disregarding additional spatially resolved land subsidence related to

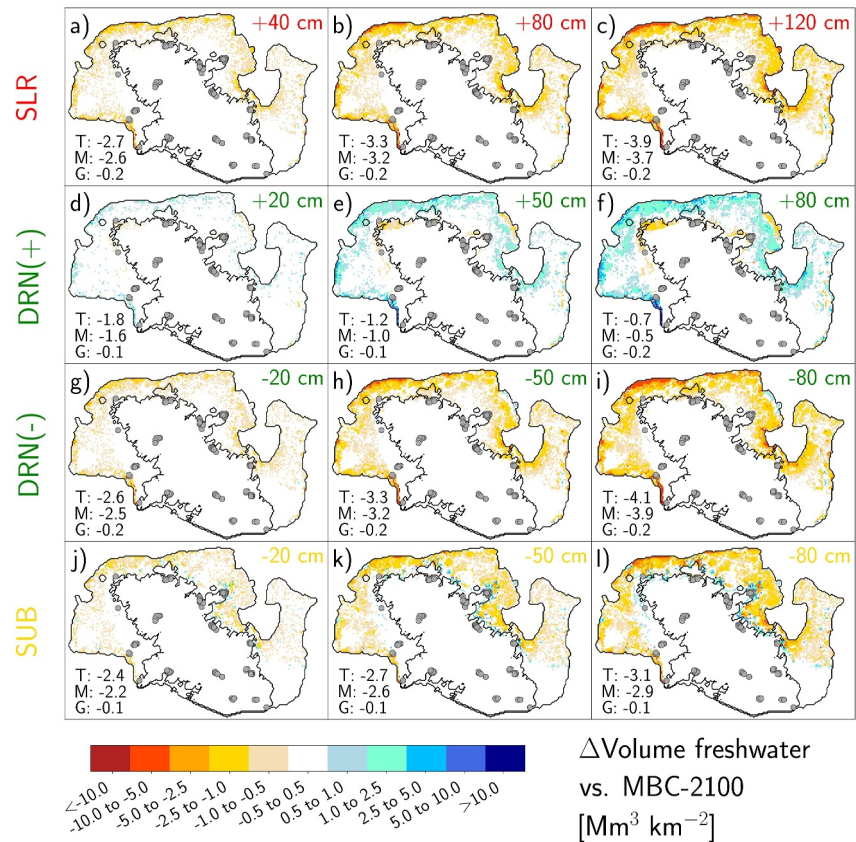


Figure 7. Change of fresh groundwater volume for selected LIN model variants at 2100 CE compared to MBC at 2100 CE. Colored numbers in the top-right corner of each subplot indicate the applied change in the respective model variant. Values in the bottom-left corner of each subplot mark the relative change of fresh groundwater volume (km^3) for the entire mainland (T), the marsh (M) and the geest (G) compared to 2020 CE.

compaction of Holocene sediments. For example, SLR was the main driver for increasing salt loads and decreasing freshwater volumes, respectively, in PRO variants (gray and green boxes in Figure 6b), because PRO variants plot close to LIN model variants exploring SLR (red dots in Figure 6b). In addition, the projected overall recharge increase, which was regarded in PRO model variants, resulted in more groundwater discharge to surface water (gray and green boxes, Figure 6a) compared to MBC (cross symbols in Figure 6a), which caused higher future salt loads in PRO model variants (i.e., vertical component of gray and green boxes in Figure 6b) compared to LIN model variants only regarding SLR (red dots in Figure 6b).

Lifting of drain elevations closer to the ground surface (green circles in Figure 6) was the only considered factor in our study that had a clear positive effect on future salinization on a regional scale. More elevated drain levels resulted in less seawater inflow (Figure 6a), counteracted the decrease of marsh fresh groundwater volume (Figures 6b and 7d–7f) and the upward movement of the freshwater interface (Figure 6c) and reduced the future salt load (Figure 6b) as well as near-surface salinities (Figure 6c).

4. Discussion

4.1. Drivers of Future Groundwater Salinization

The objectives of this study were to investigate how future climate change will affect salinization of low-lying coastal groundwater systems and to identify main salinization drivers. Firstly, we find that only the low-lying marshes of our study area are affected by future salinization, whereas freshwater reservoirs below the elevated geest landscape remain stable in our models, at least until 2100 CE. This observation agrees with Gonzalez et al. (2021), who conducted a numerical modeling study for a neighboring coastal groundwater system in Northwestern Germany. Moreover, we show that autonomous salinization, that is, salinization driven by non-equilibrium of the present-day salinity distribution with the current hydrogeological boundary conditions, is the primary salinization driver, explaining >50% of future salinization and causing a loss of ~5% of the present-day marsh fresh groundwater volume, that is, ~2,000 Mm³ freshwater, until 2100 CE in our models. The main reason for autonomous salinization is the artificial drainage of the marsh areas, which causes upward flow of saline groundwater (Oude Essink et al., 2010; Seibert et al., 2023).

Comparable salinity increases linked to autonomous salinization were reported for the central Delta region of the Netherlands (loss of <1% fresh groundwater volume and local doubling of salt loads until 2100 CE, Oude Essink et al., 2010) and the coastal region of southwestern Denmark (total model salt increase of 2% until 2200 CE, Meyer et al., 2019). The latter unconsolidated coastal groundwater systems and the here investigated site share similar hydrogeologic properties, given that they are permeable and were impacted by Pleistocene and Holocene dynamics, that is, geomorphological changes, trans- and regression periods, dike construction and extensive drainage measures linked to land cultivation (Seibert et al., 2023). Therefore, we speculate that autonomous salinization is an important driver of salinization in such low-lying coastal regions, where salinization is expected to intensify in the future regardless of projected climate change.

The demonstrated strong impact of autonomous salinization is often underestimated compared to projected SLR in coastal modeling studies, mainly because realistic initial head and salinity distributions that reflect the hydrogeological history of a low-lying coastal groundwater system are usually lacking. However, past changes, including coastline development, land surface decrease or establishment of drainage measures, can cause salinization even centuries after the corresponding change of the hydrogeological system occurred (e.g., Delsman et al., 2014), underlining that salt transport in porous media is slow, possibly resulting in a large time lag (of decennia and centuries to even millennia) between hydrogeological boundary change and saltwater intrusion. We have tackled this issue by conducting a comprehensive paleo modeling study (Seibert et al., 2023) as a first step, providing a realistic salinity distribution that resulted from important hydrogeological changes during the past 9,000 years. Although technically challenging but doable as we demonstrate, we advocate such a two-step modeling approach, that is, firstly re-constructing present-day head and salinity distributions based on comprehensive paleo modeling and, secondly, simulating future salinization integrating projected climate data. Our study highlights that this approach is key to realistically quantify the contribution of past, present and future boundary changes to salinization of most low-lying coastal groundwater systems.

SLR was the second dominant salinization driver in our models. Its impact on future salinization was almost linearly correlated with the projected rate of SLR. Thus, we conclude that low-lying coastal groundwater systems

will be affected by additional saltwater intrusion in the future because of projected SLR. Hotspot of salinity increases due to SLR is the nearshore area. The important role of SLR for future salinization was previously shown by Meyer et al. (2019), who reported that SLR of 0.85 m until 2200 CE resulted in a doubling of seawater inflow from the coastal boundary into the mainland. Main reason for the increased seawater inflow was the larger head difference between rising sea and drained marshes. Similarly, Oude Essink et al. (2010) reported that parts of the Dutch Delta aquifer are very sensitive to salinization driven by SLR. These findings agree well with our simulation results and underline that SLR will presumably force large amounts of saltwater into drained low-lying coastal groundwater systems. The role of SLR will become even more significant in the more distant future after 2100 CE, considering the projected acceleration of SLR in the next centuries (Horton et al., 2020).

Note that this study used SLR projections from Kopp et al. (2014), reflecting the state of the Special Report on the Ocean and Cryosphere in a Changing Climate by the IPCC (Oppenheimer et al., 2019), while more recent SLR projections based on the Sixth Assessment Report of the IPCC are available (IPCC, 2021). The more recent IPCC projections suggest a slightly higher total SLR in the future, for example, considering a projected SLR for tide gauge Cuxhaven of 0.48–1.42 m (5–95 percentiles of SSP5-8.5, medium confidence; Fox-Kemper et al., 2021; Garner et al., 2021; Kopp et al., 2023) versus 0.41–1.28 m (5–95 percentiles of RCP-8.5, Kopp et al., 2014) until 2100 CE. Accordingly, the effect of SLR on salinization in the investigated groundwater system is expected to be somewhat larger when taking into account the most recent SLR projections. However, because the differences between the aforementioned SLR projections are small, model results are expected to be comparable and, therefore, the discussed implications of SLR for future salinization hold true.

Land subsidence via compacting clay and peat oxidation is a further important factor controlling future salinization, which was regarded in a subset of PRO model variants. Note that we regarded the latter process by calculating spatially resolved subsidence rates of 3, 6 and 9 mm⁻¹, respectively, for all locations characterized by Holocene clay/peat/silt deposits. Thereby, spatially resolved land subsidence was combined with the comparatively low background subsidence rate of ~1 mm a⁻¹, which is lumped into the SLR projections by Kopp et al. (2014). Conceptually, land subsidence and the associated drop of inland groundwater levels correspond to an increase of relative SLR. For example, we observed that a land subsidence rate in the order of >10 mm a⁻¹ would have similar negative impacts on future salinization in our models as worst-case RCP-8.5 scenarios neglecting land subsidence. This means that marsh areas are prone to additional salinization in case of substantial land subsidence, which adds to saltwater intrusion caused by autonomous salinization and SLR. The effect of land subsidence on coastal salinization was previously demonstrated by Oude Essink et al. (2010), who incorporated projected land subsidence rates in their modeling approach for the Dutch Delta aquifer and found that land subsidence is the major salinization driver in areas characterized by Holocene clay and peat deposits. The process of land subsidence is closely related to abstraction-induced lowering of coastal groundwater levels (Minderhoud et al., 2020). Hence, the negative effects of excessive abstraction and abstraction-induced land subsidence will superimpose and put densely populated coastal areas at high risk for salinization via saltwater intrusion in the future, not to mention the increased risk of floodings for drowning coastal areas.

On the other hand, we find that the projected increase of groundwater recharge of up to ~45% of present-day recharge rates, has only a small impact on future salinization. This is because additional recharge is largely discharged to the surface water system in our models, which underlines that hydrogeology and salinity distribution of most low-lying coastal groundwater systems are heavily controlled by surface water levels and the management of the surface water system. Our findings agree with observations by Oude Essink et al. (2010), who found that a recharge surplus had only a small impact on future salinization in the central Delta region of The Netherlands, where polder water levels are artificially controlled. Yet, additional recharge may still have a positive impact on near-surface groundwater and soil salinity.

We further show that the effect of abstraction is not a substantial salinization driver in our models, at least not on a regional scale with our relatively low abstraction rates. This finding is explained by the fact that groundwater abstraction for drinking water production takes place in the elevated geest landscape. Here, groundwater recharge is sufficient to satisfy the water demand related to drinking water production. However, water works in vicinity to the marshes are more susceptible to salinization due to local saltwater upconing, particularly if abstraction rates would increase in the future. Our observations oppose the findings of previous studies, which were carried out in densely populated coastal regions. For instance, Ferguson and Gleeson (2012) employed an analytical solution to evaluate whether abstraction or SLR dominate salinization of US coastal aquifers and found that the latter were

more vulnerable to the effects of abstraction under most hydrologic conditions and population densities. Furthermore, Mabrouk et al. (2018) assessed the relative importance of groundwater abstraction and SLR, respectively, on future salinization of the Nile Delta Aquifer, Egypt, employing numerical simulations and found that abstraction was the main salinization driver. This discrepancy is likely explained by the fact that population density and, hence, abstraction volumes are relatively low in our study area. Moreover, abstraction for drinking water production is not located in the low-lying marshes, and abstraction for irrigation, at present only of minor importance, was not regarded. However, potential additional abstraction within the marsh areas in the future, for example, caused by a warmer climate and/or changes in land use, would presumably amplify salinization of the investigated groundwater system.

4.2. Implications for Coastal Water Users

Coastal water users will be facing several challenges resulting from future salinization. Firstly, salinization of the low-lying drained marsh areas will continue in the future due to autonomous salinization, regardless of future climate change. This process results in a lifting of the fresh-salt interface in most parts of the marsh, that is, on average by >3 m, which diminishes marsh fresh groundwater volumes by >5%, that is, ~2,000 Mm³ freshwater, until 2100 CE. The effects of SLR and land subsidence will further intensify the salinization process. Areas with surface elevations <0 masl are particularly sensitive to upconing of saltwater. The upwelling saline groundwater may ultimately lead to salinization of near-surface groundwater, which is a threat to the agricultural use of the affected areas. Therefore, farmers in the marshes might be forced to change crop cultivation in the future if near-surface salinities exceed plant salinity thresholds (Grieve et al., 2012). Salinization of marsh freshwater is a further issue concerning its possible use as irrigation water, which becomes pivotal for crop irrigation in a warmer climate (Wada & Bierkens, 2014), or as drinking water for cattle farming.

Moreover, coastal freshwater ecosystems are at risk due to the simulated future increase of salt discharge to surface waters. For example, benthic freshwater diatoms are affected by Cl thresholds as low as >35 mg L⁻¹ (Porter-Goff et al., 2013), and Böhme (2011) reported an increasing loss of macrozoobenthos, fish and macrophyte diversity for Cl concentrations of >400 mg L⁻¹, >750 mg L⁻¹ and >1,000 mg L⁻¹, respectively. Since the average Cl concentration of groundwater discharge to surface waters doubles from ~300 mg L⁻¹ to >600 mg L⁻¹ until 2100 CE in our models, we speculate that salinization will negatively impact the biodiversity of freshwater ecosystems in the marsh in the future, for example, as discussed by Herbert et al. (2015). Based on the findings of our representative case study, we expect that the implications of salinization for coastal water users, that is, uplifting of brackish and saline deeper groundwater in drained areas, diminishing freshwater volumes amplifying coastal water stress, and increasing near-surface groundwater salinities challenging both crop cultivation as well as coastal freshwater ecosystems, generally apply for most low-lying coastal groundwater systems in unconsolidated media. Considering that the study area is not densely populated and that abstraction volumes are comparatively low, negative implications of salinization are probably much more drastic in coastal regions with high population density.

Regarding possible countermeasures to future salinization, our study shows that increased groundwater levels in low-lying marshes due to less intensive drainage would counterbalance the hydraulic pressure associated with SLR and land subsidence, thereby mitigating saltwater intrusion. However, alleviating marsh groundwater levels would result in multiple conflicts of interest, for example, considering the limitations for agricultural use and the submersion of buildings and infrastructure associated with higher groundwater levels. Oude Essink et al. (2010) evaluated the effect of two other countermeasures on future salinization of the Dutch Delta aquifer. They found that land reclamation offshore the present-day coast resulted in the formation of a large freshwater lens, which reduced saltwater intrusion. Yet, this measure increased hydraulic heads at the coast significantly, which increased salt loads. Inundation of low-lying polder areas as second evaluated countermeasure reduced salt loads by 9% but was deemed ineffective by the authors concerning the required effort.

4.3. Limitations and Outlook

Our study has the following limitations:

- The simplified integration of the surface water and drainage system via a generalized resistance factor between groundwater and surface water systems is a major constraint. More accurate data on (seasonal) surface water levels and concentrations as well as drainage depths are needed to increase the accuracy of model predictions.

- The horizontal grid resolution of the model is relatively coarse. A finer resolution would enable the simulation of future salinization on a smaller spatial scale, yet, on the expense of increased computational costs.
- Decadal stress periods, in which boundary conditions remained constant, were used in the transient models to minimize the numerical burden, considering the large number of model variants. However, a finer temporal resolution is needed to investigate annual and seasonal effects. Particularly, the impact of the opposing trends of winter versus summer recharge, seasonal surface water level changes as well as the variation of seasonal abstraction patterns are of interest.
- Uniform land subsidence rates were assumed for all locations characterized by Holocene clay and peat in our study. The integration of spatially resolved land subsidence based on more sophisticated subsidence models would allow for a more realistic evaluation concerning the effect of land subsidence on future salinization.
- The dike line remained stable in our models. Hence, we have not regarded the effect of large-scale flooding resulting from dike failure. Because surface floodings have dramatic and long-lasting impacts on salinization of low-lying coastal areas, inclusion of such events is required to evaluate their impact on future salinization.

5. Conclusions

The objective of this study was to understand how climate change will affect future groundwater salinization in low-lying coastal groundwater systems. Moreover, the roles of individual hydrogeologic boundaries as possible salinization drivers were explored. Northwestern Germany, located at the North Sea, was selected as case study area because it shows common characteristics of unconsolidated coastal groundwater systems in Northern Europe, such as a geology dominated by permeable sands, a dynamic history of coastal evolution during the Pleistocene and Holocene as well as a hydrogeologic system that is controlled by anthropogenic measures.

Our research shows that autonomous salinization is likely the dominant salinization driver in the low-lying marshes until 2100 CE, regardless of future climate change. The more elevated geest landscape is virtually not affected by future salinization. The main reason for autonomous salinization is drainage of the low-lying marshes, resulting in groundwater levels that are artificially kept several decimeters below the ground surface. Since autonomous salinization is significant in our representative case study, we advocate a two-step modeling approach for the investigation of salinization in low-lying coastal groundwater systems, that is, firstly re-constructing present-day salinity distributions via paleo modeling and, secondly, forcing models with climate data, applying re-constructed salinity distributions as initial conditions. Climate change amplifies the salinization process, with SLR being the dominant factor causing saltwater intrusion in the future besides autonomous salinization. Because SLR is expected to further accelerate in the future, SLR will likely become the main driver of future groundwater salinization in the long run, that is, after 2100 CE. Moreover, our study demonstrates that land subsidence related to compaction of Holocene clay/peat/silt deposits can become a key factor driving future groundwater salinization. The impact of changing groundwater recharge and abstraction is less pronounced but will likely put stress to agriculture and soils.

The simulated future salinization trends have severe implications for coastal water users. Salinization of near-surface groundwater will affect agricultural use and may require different crop cultivation in the future. Furthermore, increasing salt loads will raise surface water salinities, putting the diversity of freshwater ecosystems under increasing pressure and crop irrigation with surface water at risk. To conclude, our study demonstrates that autonomous salinization, SLR and land subsidence are dominant salinization drivers in the investigated representative low-lying coastal groundwater system and, therefore, should be considered when investigating salinization in other coastal regions. The here presented modeling approach may serve as blueprint for this purpose. Future research should be directed toward evaluating the efficiency of possible countermeasures to support the development of coastal adaptation strategies.

Conflict of Interest

The authors declare no conflicts of interest relevant to this study.

Data Availability Statement

Model input/output data of the numerical models, iMOD-Python (Visser & Bootsma, 2019) scripts to create model input files for each model variant as well as Python scripts to create the figures presented in this article are

available on the Zenodo repository (Seibert et al., 2024). iMOD-WQ used for running the numerical simulations has been made available by Deltares (2020), as described by Verkaik et al. (2021). iMOD-Python used to create input files to the numerical models is available via <https://gitlab.com/deltares/imod/imod-python>.

Acknowledgments

We thank the following institutions for manifold support: Deltares (technical modeling support), Landesamt für Bergbau, Energie und Geologie (LBEG) and Niedersächsisches Kompetenzzentrum Klimawandel (NIKO) (provision of mGROWA18/22, geologic and freshwater interface data), Niedersächsischer Landesbetrieb für Wasserwirtschaft, Küsten- und Naturschutz (NLWKN) (provision of groundwater heads/salinities, river levels/discharges), Oldenburg-Ostfriesischer Wasserverband (OOWV) (provision of geologic data and abstraction rates) as well as regional water works (provision of abstraction rates). We thank L. Karrasch and B. Siebenhüner for fruitful collaboration within the SALTSA project. Simulations were performed at the University of Oldenburg HPC Cluster ROSA, located at the University of Oldenburg (Germany) and funded by the DFG through its Major Research Instrumentation Programs (INST 184/225-1 FUGG) and the Ministry of Science and Culture (MWK) of the Lower Saxony State. The DFG is thanked for SALTSA project funding (MA 3274/9-1) within the Special Priority Programme (SPP-1889) "Regional Sea Level Change and Society (SeaLevel)." Research related to this article further benefited from funding of the projects WAKOS (BMBF; support code 01LR2003E) and the DFG research unit FOR 5094: The dynamic deep subsurface of high-energy beaches (DynaDeep) (GR 4514/3-1). Open Access funding enabled and organized by Projekt DEAL.

References

- Ataie-Ashtiani, B., Werner, A. D., Simmons, C. T., Morgan, L. K., & Lu, C. (2013). How important is the impact of land-surface inundation on seawater intrusion caused by sea-level rise? *Hydrogeology Journal*, 21(7), 1673. <https://doi.org/10.1007/s10040-013-1021-0>
- Bhuiyan, M. J. A. N., & Dutta, D. (2012). Assessing impacts of sea level rise on river salinity in the Gorai river network, Bangladesh. *Estuarine, Coastal and Shelf Science*, 96, 219–227. <https://doi.org/10.1016/j.ecss.2011.11.005>
- Böhme, D. (2011). Evaluation of brine discharge to rivers and streams: Methodology of rapid impact assessment. *Limnologia*, 41(2), 80–89. <https://doi.org/10.1016/j.limno.2010.08.003>
- Bundesamt für Kartographie und Geodäsie (BKG) [Federal Agency for Cartography and Geodesy]. (2013). Digitales Geländemodell Gitterweite 200 m – DGM200. Data received in 2017.
- Cantelon, J. A., Guimond, J. A., Robinson, C. E., Michael, H. A., & Kurylyk, B. L. (2022). Vertical saltwater intrusion in coastal aquifers driven by episodic flooding: A review. *Water Resources Research*, 58(11), 1–25. <https://doi.org/10.1029/2022WR032614>
- Colombani, N., Mastrocicco, M., & Giambastiani, B. M. S. (2015). Predicting salinization trends in a lowland coastal aquifer: Comacchio (Italy). *Water Resources Management*, 29, 603–618. <https://doi.org/10.1007/s11269-014-0795-8>
- De Louw, P. G., Oude Essink, G. H. P., Stuyfzand, P. J., & Van der Zee, S. E. A. T. M. (2010). Upward groundwater flow in boils as the dominant mechanism of salinization in deep polders, The Netherlands. *Journal of Hydrology*, 394(3–4), 494–506. <https://doi.org/10.1016/j.jhydrol.2010.10.009>
- Delsman, J. R., Hu-A-Ng, K. R. M., Vos, P. C., de Louw, P. G., Oude Essink, G. H. P., Stuyfzand, P. J., & Bierkens, M. F. (2014). Paleo-modeling of coastal saltwater intrusion during the Holocene: An application to The Netherlands. *Hydrology and Earth System Sciences*, 18(10), 3891–3905. <https://doi.org/10.5194/hess-18-3891-2014>
- Deltares. (2020). iMOD 5.2: iMOD-WQ (water quality) [Software]. <https://oss.deltares.nl/web/imod>
- Deutscher Wetterdienst (DWD) [German Meteorological Service]. (2021). Climate Data for the model region [Dataset]. Retrieved from the CDC-Portal https://opendata.dwd.de/climate_environment/
- Doherty, J. E. (2021a). *PEST model-independent parameter estimation user manual Part I: PEST, SENSAN and global optimisers* (p. 394). Watermark Numerical Computing.
- Doherty, J. E. (2021b). *PEST model-independent parameter estimation user manual Part II: PEST utility support software* (p. 274). Watermark Numerical Computing.
- Döll, P. (2009). Vulnerability to the impact of climate change on renewable groundwater resources: A global-scale assessment. *Environmental Research Letters*, 4(3), 035006. <https://doi.org/10.1088/1748-9326/4/3/035006>
- Ertl, G., Bug, J., Elbracht, J., Engel, N., & Herrmann, F. (2019). Grundwasserneubildung von Niedersachsen und Bremen - Berechnungen mit dem Wasserhaushaltsmodell mGROWA18. *GeoBerichte*, 36.
- Eslami, S., Hoekstra, P., Nguyen Trung, N., Ahmed Kantoush, S., Van Binh, D., Duc Dung, D., et al. (2019). Tidal amplification and salt intrusion in the Mekong Delta driven by anthropogenic sediment starvation. *Scientific Reports*, 9(1), 1–10. <https://doi.org/10.1038/s41598-019-55018-9>
- Ferguson, G., & Gleeson, T. (2012). Vulnerability of coastal aquifers to groundwater use and climate change. *Nature Climate Change*, 2(5), 342–345. <https://doi.org/10.1038/nclimate1413>
- Feseker, T. (2007). Numerical studies on saltwater intrusion in a coastal aquifer in northwestern Germany. *Hydrogeology Journal*, 15(2), 267–279. <https://doi.org/10.1007/s10040-006-0151-z>
- Fox-Kemper, B., Hewitt, H. T., Xiao, C., Aðalgeirsdóttir, G., Drijfhout, S. S., Edwards, T. L., et al. (2021). Ocean, cryosphere and sea level change. In V. Masson-Delmotte, P. Zhai, A. Pirani, S. L. Connors, C. Péan, S. Berger, et al. (Eds.), *Climate change 2021: The physical science basis. Contribution of working group I to the sixth assessment report of the intergovernmental panel on climate change* (pp. 1211–1362). Cambridge University Press. <https://doi.org/10.1017/9781009157896.011>
- Garner, G. G., Hermans, T., Kopp, R. E., Slangen, A. B. A., Edwards, T. L., Levermann, A., et al. (2021). IPCC AR6 sea-level rise projections. Version 20210809. PO.DAAC, CA, USA. Retrieved from <https://sealevel.nasa.gov/ipcc-ar6-sea-level-projection-tool>
- González, E., Deus, N., Elbracht, J., Azizur Rahman, M., & Wiederhold, H. (2021). Current and future state of groundwater salinization of the northern Elbe-Weser region. *Grundwasser*, 26(4), 343–356. <https://doi.org/10.1007/s00767-021-00496-w>
- Green, N. R., & Macquarrie, B. (2014). An evaluation of the relative importance of the effects of climate change and groundwater extraction on seawater intrusion in coastal aquifers in Atlantic Canada. *Hydrogeology Journal*, 22(3), 609. <https://doi.org/10.1007/s10040-013-1092-y>
- Grieve, C. M., Grattan, S. R., & Maas, E. V. (2012). Plant salt tolerance. ASCE manual and reports on engineering practice, 71, 405–459.
- Hajati, M., Harders, D., Petry, U., Elbracht, J., & Engel, N. (2022). Dokumentation der niedersächsischen Klimaprojektionsdaten AR5-NI v2.1. Geofakt 39, Landesamt für Bergbau, Energie und Geologie, Hannover, Germany. https://doi.org/10.48476/geofakt_39_1_2022
- Harbaugh, A. W., Banta, E. R., Hill, M. C., & McDonald, M. G. (2000). Modflow-2000, the U.S. Geological Survey modular ground-water model-user guide to modularization concepts and the ground-water flow process. Open-file report (Vol. 92, p. 134). U. S. Geological Survey.
- Herbert, E. R., Boon, P., Burgin, A. J., Neubauer, S. C., Franklin, R. B., Ardón, M., et al. (2015). A global perspective on wetland salinization: Ecological consequences of a growing threat to freshwater wetlands. *Ecosphere*, 6(10), 1–43. <https://doi.org/10.1890/ES14-00534.1>
- Herrera-García, G., Ezquerro, P., Tomás, R., Béjar-Pizarro, M., López-Vinielles, J., Rossi, M., et al. (2021). Mapping the global threat of land subsidence. *Science*, 371(6524), 34–36. <https://doi.org/10.1126/science.abb8549>
- Herrmann, F., Chen, S., Heidt, L., Elbracht, J., Engel, N., Kunkel, R., et al. (2013). Zeitlich und räumlich hochaufgelöste flächendifferenzierte Simulation des Landschaftswasserhaushalts in Niedersachsen mit dem Model mGROWA. *Hydrologie und Wasserbewirtschaftung*, 57(5), 206–224. https://doi.org/10.5675/HyWa_2013.5_2
- Holt, T., Seibert, S. L., Greskowiak, J., Freund, H., & Massmann, G. (2017). Impact of storm tides and inundation frequency on water table salinity and vegetation on a juvenile barrier island. *Journal of Hydrology*, 554, 666–679. <https://doi.org/10.1016/j.jhydrol.2017.09.014>
- Horton, B. P., Khan, N. S., Cahill, N., Lee, J. S., Shaw, T. A., Garner, A. J., et al. (2020). Estimating global mean sea-level rise and its uncertainties by 2100 and 2300 from an expert survey. *Climate and Atmospheric Science*, 3(1), 18. <https://doi.org/10.1038/s41612-020-0121-5>
- Illangasekare, T., Tyler, S. W., Clement, T. P., Villholth, K. G., Perera, A. P. G. R. L., Obeysekera, J., et al. (2006). Impacts of the 2004 tsunami on groundwater resources in Sri Lanka. *Water Resources Research*, 42(5). <https://doi.org/10.1029/2006WR004876>

- IPCC. (2021). Climate change 2021: The physical science basis. In V. Masson-Delmotte, P. Zhai, A. Pirani, S. L. Connors, C. Péan, et al. (Eds.), *Contribution of working group I to the Sixth assessment Report of the intergovernmental panel on climate change* (p. 2391). Cambridge University Press. <https://doi.org/10.1017/9781009157896>
- Karle, M., Bungenstock, F., & Wehrmann, A. (2021). Holocene coastal landscape development in response to rising sea level in the Central Wadden Sea coastal region. *Netherlands Journal of Geosciences*, 100. <https://doi.org/10.1017/njg.2021.10>
- Karrasch, L., Siebenhüner, B., & Seibert, S. L. (2023). Groundwater salinization in northwestern Germany: A case of anticipatory governance in the field of climate adaptation? *Earth System Governance*, 17, 100179. <https://doi.org/10.1016/j.esg.2023.100179>
- Kopp, R. E., Garner, G. G., Hermans, T. H. J., Jha, S., Kumar, P., Reedy, A., et al. (2023). The framework for assessing changes to sea-level (FACTS) v1.0: A platform for characterizing parametric and structural uncertainty in future global, relative, and extreme sea-level change. *Geoscientific Model Development*, 16, 7461–7489. <https://doi.org/10.5194/gmd-16-7461-2023>
- Kopp, R. E., Horton, R. M., Little, C. M., Mitrovica, J. X., Oppenheimer, M., Rasmussen, D. J., et al. (2014). Probabilistic 21st and 22nd century sea-level projections at a global network of tide-gauge sites. *Earth's Future*, 2(8), 383–406. <https://doi.org/10.1002/2014EF000239>
- Landesamt für Bergbau, Energie und Geologie (LBEG) [State Office for Mining, Energy and Geology]. (2018). Geologic models for the East-Frisian regions Nordenham and Varel. Data provided in, 2018.
- Landesamt für Bergbau, Energie und Geologie (LBEG) [State Office for Mining, Energy and Geology] & Niedersächsisches Kompetenzzentrum Klimawandel (NIKO) [Lower Saxony Competence Center for Climate Change]. (2022). Grundwasserneubildung für die Klimaszenarien-Zeiträume (Methode: mGROWA22) – NIBIS® Kartenserver im Niedersächsischen Bodeninformationssystem [Dataset]. Retrieved from <http://nibis.lbeg.de/cardomap3/>
- Langevin, C. D., Thorne, D. T., Jr., Dausman, A. M., Sukop, M. C., & Guo, W. (2008). *SEAWAT version 4: A computer program for simulation of multi-species solute and heat transport (No. 6-A22)*. Geological Survey (US).
- Mabrouk, M., Jonoski, A., Oude Essink, G. H. P., & Uhlenbrook, S. (2018). Impacts of sea level rise and groundwater extraction scenarios on fresh groundwater resources in the Nile Delta Governorates, Egypt. *Water*, 10(11), 1690. <https://doi.org/10.3390/w10111690>
- Meyer, R., Engesgaard, P., & Sonnenborg, T. O. (2019). Origin and dynamics of saltwater intrusion in a regional aquifer: Combining 3-D saltwater modeling with geophysical and geochemical data. *Water Resources Research*, 55(3), 1792–1813. <https://doi.org/10.1029/2018WR023624>
- Michael, H. A., Russoniello, C. J., & Byron, L. A. (2013). Global assessment of vulnerability to sea-level rise in topography-limited and recharge-limited coastal groundwater systems. *Water Resources Research*, 49(4), 2228–2240. <https://doi.org/10.1002/wrcr.20213>
- Minderhoud, P. S. J., Middelkoop, H., Erkens, G., & Stouthamer, E. (2020). Groundwater extraction may drown mega-delta: Projections of extraction-induced subsidence and elevation of the Mekong delta for the 21st century. *Environmental Research Communications*, 2(1), 011005. <https://doi.org/10.1088/2515-7620/ab5e21>
- Nicholls, R. J., Lincke, D., Hinkel, J., Brown, S., Vafeidis, A. T., Meyssignac, B., et al. (2021). A global analysis of subsidence, relative sea-level change and coastal flood exposure. *Nature Climate Change*, 45(7), 634. <https://doi.org/10.1038/s41558-021-00993-z>
- Niedersächsischer Landesbetrieb für Wasserwirtschaft, Küsten- und Naturschutz (NLWKN) [Lower Saxony Water Management, Coastal Defence and Nature Conservation Agency]. (2016). Fließgewässer (WRRLL) Niedersachsen. Data received in 2017.
- Oldenburg-Ostfriesischer Wasserverband (OOWV) [Oldenburg-East Frisian Water Board]. (2020). Geologic model for the German East-Frisian region. Data received in 2020.
- Oppenheimer, M., Glavovic, B., Hinkel, J., van de Wal, R., Maignan, A. K., Abd-Elgawad, A., et al. (2019). Chapter 4: Sea level rise and implications for low lying islands, coasts and communities. In *IPCC special report on the ocean and cryosphere in a changing climate* (pp. 321–445). Cambridge University Press. <https://doi.org/10.1126/science.aam6284>
- Oude Essink, G. H. P. (2001). Saltwater intrusion in a three-dimensional groundwater system in The Netherlands: A numerical study. *Transport in Porous Media*, 43, 137–158. <https://doi.org/10.1023/A:1010625913251>
- Oude Essink, G. H. P., Van Baaren, E. S., & De Louw, P. G. (2010). Effects of climate change on coastal groundwater systems: A modeling study in The Netherlands. *Water Resources Research*, 46(10). <https://doi.org/10.1029/2009WR008719>
- Paldor, A., & Michael, H. A. (2021). Storm surges cause simultaneous salinization and freshening of coastal aquifers, exacerbated by climate change. *Water Resources Research*, 57(5), 1–14. <https://doi.org/10.1029/2020WR029213>
- Porter-Goff, E. R., Frost, P. C., & Xenopoulos, M. A. (2013). Changes in riverine benthic diatom community structure along a chloride gradient. *Ecological Indicators*, 32, 97–106. <https://doi.org/10.1016/j.ecolind.2013.03.017>
- Portmann, F. T., Döll, P., Eisner, S., & Flörke, M. (2013). Impact of climate change on renewable groundwater resources: Assessing the benefits of avoided greenhouse gas emissions using selected CMIP5 climate projections. *Environmental Research Letters*, 8(2), 024023. <https://doi.org/10.1002/2014WR015595>
- Reutter, E., Landesamt für Bergbau, Energie und Geologie (LBEG) [State Office for Mining, Energy and Geology]. (2013). Hydrostratigrafische Gliederung Niedersachsens. Geofakten 21, Landesamt für Bergbau, Energie und Geologie, Hannover, Germany.
- Seibert, S. L., Greskowiak, J., Bungenstock, F., Freund, H., Karle, M., Meyer, R., et al. (2023). Paleo-hydrogeological modeling to understand present-day groundwater salinities in a low-lying coastal groundwater system (northwestern Germany). *Water Resources Research*, 59(4), e2022WR033151. <https://doi.org/10.1029/2022WR033151>
- Seibert, S. L., Greskowiak, J., Oude Essink, G. H. P., & Massmann, G. (2024). Research data related to the article “Understanding climate change and anthropogenic impacts on the salinization of low-lying coastal groundwater systems” (v1.0.0) [Dataset]. *Earth's Future*. Zenodo. <https://doi.org/10.5281/zenodo.12607668>
- Seibert, S. L., Holt, T., Reckhardt, A., Ahrens, J., Beck, M., Pollmann, T., et al. (2018). Hydrochemical evolution of a freshwater lens below a barrier island (Spiekeroog, Germany): The role of carbonate mineral reactions, cation exchange and redox processes. *Applied Geochemistry*, 92, 196–208. <https://doi.org/10.1016/j.apgeochem.2018.03.001>
- Shirzaei, M., Freymueller, J., Törnqvist, T. E., Galloway, D. L., Dura, T., & Minderhoud, P. S. (2021). Measuring, modelling and projecting coastal land subsidence. *Nature Reviews Earth & Environment*, 2(1), 40–58. <https://doi.org/10.1038/s43017-020-00115-x>
- Small, C., & Nicholls, R. J. (2003). A global analysis of human settlement in coastal zones. *Journal of Coastal Research*, 19(3), 584–599.
- Smith, A. J., & Turner, J. V. (2001). Density-dependent surface water-groundwater interaction and nutrient discharge in the Swan-Canning Estuary. *Hydrological Processes*, 15(13), 2595–2616. <https://doi.org/10.1002/hyp.303>
- Tiggeloven, T., De Moel, H., Winsemius, H. C., Eilander, D., Erkens, G., Gebremedhin, E., et al. (2020). Global-scale benefit-cost analysis of coastal flood adaptation to different flood risk drivers using structural measures. *Natural Hazards and Earth System Sciences*, 20(4), 1025–1044. <https://doi.org/10.5194/nhess-20-1025-2020>
- Van Engelen, J., Oude Essink, G. H. P., & Bierkens, M. F. P. (2022). Sustainability of fresh groundwater resources in fifteen major deltas around the world. *Environmental Research Letters*, 17(12), 125001. <https://doi.org/10.1088/1748-9326/aca16c>

- Van Engelen, J., Verkaik, J., King, J., Nofal, E. R., Bierkens, M. F. P., & Oude Essink, G. H. P. (2019). A three-dimensional palaeohydrogeological reconstruction of the groundwater salinity distribution in the Nile Delta Aquifer. *Hydrology and Earth System Sciences*, 23(12), 5175–5198. <https://doi.org/10.5194/hess-23-5175-2019>
- Verkaik, J., Hughes, J. D., van Walsum, P. E. V., Oude Essink, G. H. P., Lin, H. X., & Bierkens, M. F. P. (2021). Distributed memory parallel groundwater modeling for The Netherlands Hydrological Instrument. *Environmental Modelling & Software*, 143, 105092. <https://doi.org/10.1016/j.envsoft.2021.105092>
- Vineis, P., Chan, Q., & Khan, A. E. (2011). Climate change impacts on water salinity and health. *Journal of Epidemiology and Global Health*, 1(1), 5–10. <https://doi.org/10.1016/j.jegh.2011.09.001>
- Visser, M., & Bootsma, H. (2019). iMOD-Python: Work with iMOD MODFLOW models in Python. Retrieved from <https://imod.xyz/>
- Wada, Y., & Bierkens, M. F. P. (2014). Sustainability of global water use: Past reconstruction and future projections. *Environmental Research Letters*, 9(10), 104003. <https://doi.org/10.1088/1748-9326/9/10/104003>
- Werner, A. D., Bakker, M., Post, V. E. A., Vandenbohede, A., Lu, C., Ataie-Ashtiani, B., et al. (2013). Seawater intrusion processes, investigation and management: Recent advances and future challenges. *Advances in Water Resources*, 51, 3–26. <https://doi.org/10.1016/j.advwatres.2012.03.004>
- Zamrsky, D., Oude Essink, G. H. P., & Bierkens, M. F. P. (2024). Global impact of sea level rise on coastal fresh groundwater resources. *Earth's Future*, 12(1). <https://doi.org/10.1029/2023EF003581>
- Zheng, C., & Wang, P. P. (1999). MT3DMS: A modular three-dimensional multispecies transport model for simulation of advection, dispersion, and chemical reactions of contaminants in groundwater systems; documentation and user's guide.